JOURNAL OF OPTOELECTRONICS AND ADVANCED MATERIALS, Vol. 10, No. 9, September 2008, p. 2199 - 2204

Invited Paper

Fabrication of 3D metallic micro/nanostructures by two-photon absorption

N. TOSA[a, c, d], G. VITRANT[b], P.L. BALDECK[a], O. STEPHAN[a], I. GROSU[d]
[a]*Laboratoire de Spectrométrie Physique, Université Joseph Fourier, CNRS, BP 87, 38402 Saint Martin d'Hères, France*
[b]*IMEP-LAHC, MINATEC, INPG-CNRS-UJF, BP 257, 38016 Grenoble, France*
[c]*National Institute for R&D of Isotopic and MolecularTechnologies,RO 400293 Cluj-Napoca, Romania*
[d]*Babes-Bolyai University, Organic Chemistry Department, RO 400028 Cluj-Napoca, Romania*

We report on the fabrication of three-dimensional gold structures by two-photon absorption (TPA) reduction of gold salt, dispersed in a polymer host. In this work we developed an efficient method that overcomes the thermal effect pointed out by the double-line obtained by TPA reduction in solid thin films. We show that optimized experimental conditions allow us to generate a metallic single wire deposition, and to fabricate regular and well-defined 3D gold microstructure embedded in a dielectric matrix. This direct 3D controlled metal photo-deposition procedure may be useful to create diffraction gratings with spectral filtering properties.

(Received February 25, 2008; accepted August 25, 2008)

Keywords: Two-photon absorption, thermal effect, single nanowire, 3D gold structures

1. Introduction

Two-photon induced photochemistry is based on two-photon absorption (TPA) process and represents an advanced method to obtain one-dimensional (1D), two-dimensional (2D) and three-dimensional (3D) micro/nanostructured materials such as polymers, proteins and metals. The main aspect consists in the spatial confinement of the chemical process in a small volume at the laser focal point. In spite of this advantage, the first attempts have been done only in 1992 [1] on some resins used in microelectronics. Five years later, TPA technique started to be successfully applied for 3D polymer structures fabrication [2-4], through a radical mechanism. However, lesser attempts were reported for metals, particularly for noble metals such as gold and silver, since their nanoparticles generation was highly developed by many techniques due to their great interest in fields such as electronics, photonics, optical and biological sensing [5, 6].

Three-dimensional structures such as spirals consisting of discrete silver particles were obtained by using a photographic-like approach within a silver doped sol-gel dielectric matrix [7]. The 3D latent image was generated by a femtosecond pulse inside the photographic medium thanks to a high numerical aperture objective use and remained inside the matrix after the final fixing step. Also, the laser- and electron-beam induced photo-reductive growth of 2D and 3D metallic structures within a solid matrix or on ITO substrate has been reported [8]. The solid matrix contained an appropriate dye-attached [9] on nanoparticles, which induced the photo-reduction process, as well as ligand-coated metal nanoparticles [10] as seeds to favor the particles growth. TPA ion reduction within aqueous solution of metal salts required increased laser powers in order to achieve 3D silver conductive structures [11]. A multi-step approach for 3D fabrication of metamaterials micro/nanostructures [12] has been proposed by combining the two-photon polymerization (TPP) technique to fabricate 3D structures [13] with electroless plating (EP) process to coat them selectively with metal [14].

It is also noteworthy that recently we have successfully fabricated continuous 1D and 2D gold structures by TPA [15] which exhibit diffraction properties when observed in dark-field [16]. In view of these, we considered important to investigate the feasibility of 3D structures achievement by TPA using the aqueous polymeric system already employed [17]. In this paper we focused on the optimized experimental conditions which allowed us to generate a metallic single wire deposition, and to fabricate regular and well-defined parameters 3D gold microstructure embedded in a dielectric matrix. In addition, we report on possible applications of such structures as photonic band gap devices with spectral filters properties.

2. Experimental

The metallic structures were fabricated by using an aqueous solution that contains the active compounds. Chemicals such as tetrachloroauric acid were purchased from Aldrich and used as received. As support were employed microscope glass plates (25 x 25 mm), heated in iso-propanol for 30 minutes and dried under nitrogen flow before use. The cleaned slides were then coated with a

polyimide thin layer of 900 nm, to increase the attachment of gold structures on substrate [18].

The aqueous solutions were freshly prepared before use, using equal parts of two stable solutions, denoted A and B. Solution A was prepared by dissolving various amounts of gold salt in 1mL of poly(4-styrenesulfonic acid) 18 wt. % in H_2O, denoted PSS. Solution B was prepared by dissolving $2.9 \cdot 10^{-2}$ mMol ammonium ferric citrate green in 1 mL PSS. In this view, were prepared several chemical systems containing the active species dispersed into PSS. Thus, the gold salt was varied in a range from $5 \cdot 10^{-4}$M to $0.625 \cdot 10^{-4}$M, while the ammonium ferric citrate concentration was maintained at $2.9 \cdot 10^{-5}$M (solutions 1-4).

Thick films were prepared by depositing a droplet from aqueous solution on microscope slides. Thin solid films were prepared by spin-coating (3000 rpm) from aqueous solution deposited on polyimide underlayered glass slides. The films were then placed in a three-axis microscope stage, controlled by a computer, allowing their translation relative to the focal point, with a given speed.

A femtosecond Ti: Sapphire laser (λ= 740 nm) was used to fabricate the metallic structures. The laser pulse has a duration of 100 fs and a repetition rate of 82 MHz, with average powers of about few tens of miliwatts. The laser beam was directed into an inverted microscope (Carl Zeiss Axiovert 200) by using an x100 oil-immersion objective lens (NA 1.25) to focus the laser beam within the sample.

Following «writing» the gold structures, the unreacted polymer matrix is removed by washing with iso-propanol and ethanol. No deposition of metal was observed at any laser intensity when the laser was not mode-locked, which points out the multiphoton nature of the photo-reduction process.

UV-Vis spectra in thin solid films were recorded on a Perkin Elmer Lambda 25 UV-Visible spectrometer in the range from 200nm to 1000 nm. Optical images were recorded both in transmission under normal incidence and in "dark-field", respectively. Optical scattering (transmission under normal incidence) have been obtained by sampling the image plane with an optical fiber connected to a spectrometer.

AFM measurements were performed on a Veeco 3100 scanning probe microscope with a Si_2N_4 tip, using the "tapping mode".

3. Results and discussion

3.1 UV-Vis spectra in solid state

Preliminary UV-Visible spectra measurements were performed in thin films, deposited from solutions containing various Au(III): ammonium Fe(III) citrate ratios, in order to choose the proper chemical composition of the desire environment matrix for 3D metal fabrication.

Figure 1(a) illustrates UV-Vis spectra recorded in thin films, deposited from solution 1 to 4, which show absorption peaks located at 320 nm, assigned to Au (III) specie. The absorption peak intensities are proportional to the gold salt concentrations, except spectrum 1 where the absorption peak intensity is similar to spectrum 2. This effect can be explained by the chemical reaction between gold salt and ammonium ferric citrate prior to irradiation, which generates low amounts of gold clusters undetectable in spectrum.

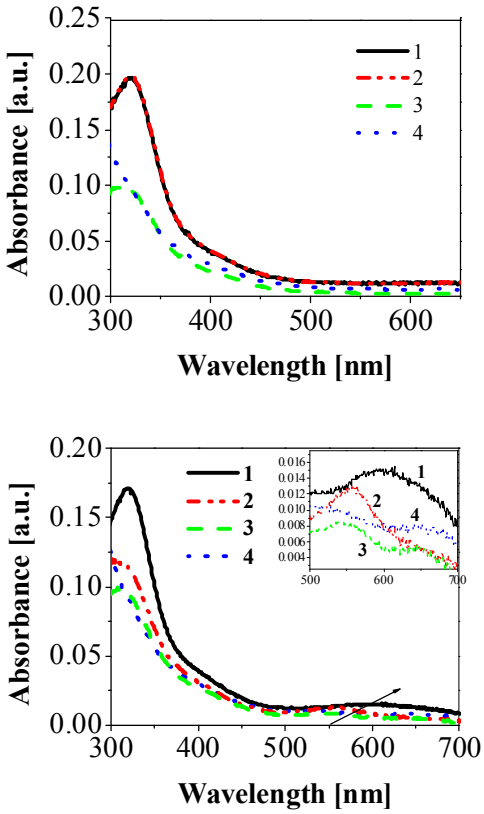

Fig. 1 Evolution of UV-Vis spectra recorded at different gold salt concentrations (a) before and (b) after 20 minutes UV irradiation. The gold concentrations corresponding to solutions 1-4 are as following: $5 \cdot 10^{-4}$M, $2.5 \cdot 10^{-4}$M, $1.25 \cdot 10^{-4}$M, and $0.625 \cdot 10^{-4}$M.

Fig. 1(b) shows absorption spectra recorded after 20 minutes UV irradiation. The appearance of weak plasmon peaks around 550 nm, coupled with the decrease of bands at 320 nm, indicates the nanoparticles generation through photo-reduction process. The signal is less broad and shows low intensities, dealing with the diffusion of active species in solid state, that is slower than in solution [17]. On the other hand, the gradual broadening and the red-shifting of plasmon peak position (especially curve 1) are induced by the increasingly gold salt: ammonium ferric citrate ratio, and clearly illustrate the growth of gold nanoparticles during UV irradiation.

3.2 Nucleation and growth

How can we control the cluster generation, and further the growth of metallic structures, when the energy provided by laser irradiation is considerably lower than the

UV one but highly localized within the gold salt- doped matrix?

Figs. 2(a) and 2(b) present a very simple experiment, performed in order to illustrate the process. In this direction, two lines were "written" in a solid thin film: a horizontal line, and then a vertical one, starting from the end of the first. An additional vertical wire, that crosses the horizontal one, allows a certain interaction of the laser beam with nanoparticles already formed and comes to confirm the nature of the process. The fabricated lines are very sensitive to the writing conditions. At low laser power the lines are thin and show granular structure, as shown in Figure 2(a). On the contrary, at higher power the lines are regular, but exhibit a double-wire shape due to the ablation process, which occurs immediately after laser interaction with gold nanoparticles previously formed – Fig. 2(b).

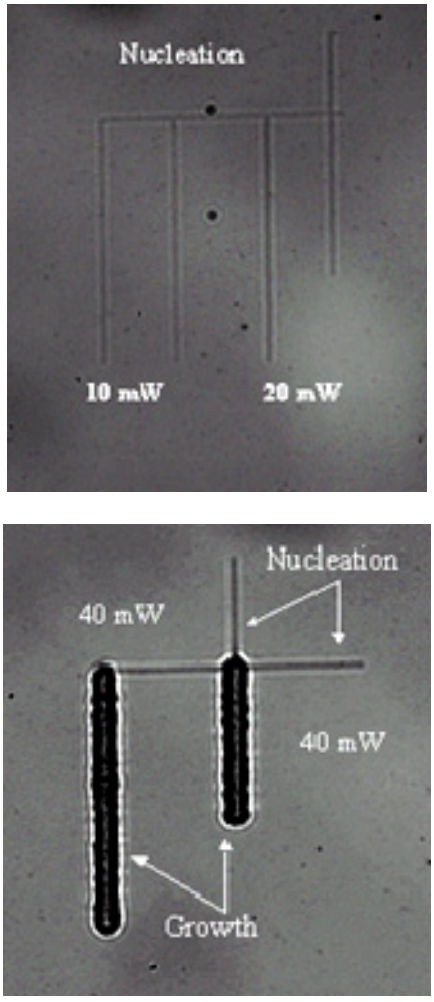

Fig. 2 Competition between (a) nucleation and (b) growth processes during the gold photo-reduction in thin film, at different laser powers

The increase of energy may induce a competition between two processes: generation of new nucleation centres, and growth of already formed particles, the last one being favoured because it requires less energy than nucleation. The growth process is favoured by the presence of metal nucleation centres, only when the laser energy is high enough to start it. Figure 2(a) shows that low powers, such as 10mW or 20 mW, did not induce the growth process, although the laser beam interacts with already generated gold nanoparticles. On the contrary, when the laser power increases at 40 mW, the laser beam interacts with nucleation centers, and rapidly induces the growth process. The wires size, deposited during the growth process, is significantly bigger compared with those obtained through the nucleation one.

The photo-reduction of gold salt complex, situated at the bright laser spot area, gain energy by TPA irradiation and lead to elemental gold nanoparticles as hard cores clothed in the soft host matrix. The small hydrophobic gold clusters pack together and form stable nanostructures due to the interparticles van der Waals forces. A higher concentration of gold colloids into polymer matrix, combined with complete (or almost complete) evaporation of the solvent in its thin film, lead to regular shape of the wires [15]. The lack of solvent arises locally the temperature and favours the metal deposition. The temperature gradients, resulting from a less uniform local laser-induced heating of the film as well as of the gold deposit itself during the photo-reduction, may induce an additional ablation process, which generates the double-wire shape.

The above experiment, associated with absorption spectra in solid state, suggested us an "optimum" of experimental conditions which can lead to good quality lines without ablation. For our case a laser power of 15 mW and a gold salt concentration of $2.5 \cdot 10^{-5}$ M proved to yield the best quality of the lines.

3.3 Single wire

Fig. 3(a) presents a serie of gold lines, fabricated in fresh thick film, with respect to "optimum" conditions presented above. The translation speed of the microscope stage was varied in the range of 2.0-5.0 μm/s, at a delay time (DT) of 5 ms. After "writing" the structures, the unreacted matrix was removed by washing with iso-propanol and ethanol, leaving on substrate one-single wires, surrounded by air, as shown in Figure 3(b). We must point out that these experimental conditions allowed us to overcome the thermal effect previously described [15]. The chemical composition of polymer host plays an important role in process. Thus, the high boiling points of solvents, in our case water, can take over the additional heat in the droplet and overcome the ablation of gold deposits, which generates the metallic double-wire shape. Also, the wires inhomogeneity induced by the bubbles produced within the film can be avoided.

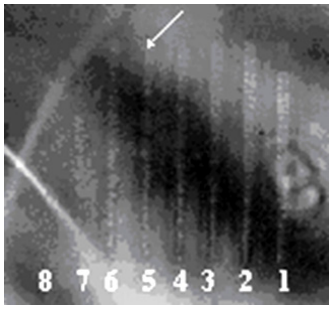

a

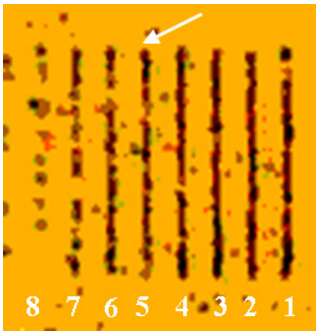

b

Fig. 3. Optical images of one-single gold wires deposited in thick film, recorded in transmitted light: (a) in polymer matrix; (b) surrounded by air, after washing process.

Fig. 4(a) shows typical AFM measurements of the fifth line described in Fig. 3, recorded at 14 mW laser power and 4 μm/s speed. They evidence a full width at half maximum (FWHM) of 480 nm, total width of 875 nm and height of 140 nm (measured on averaged section).

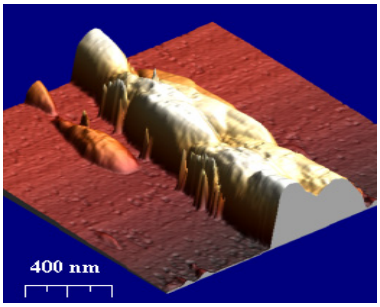

a

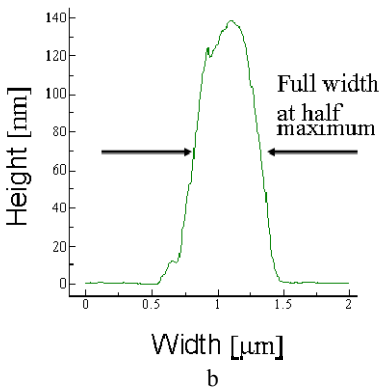

b

Fig. 4. Typical AFM measurements for a gold single wire: (a) 3D view and (b) cross-section.

Fig. 5 shows the dependence of wires FWHM on the scanning speed during the metal laser writing process. It evidences a decrease of FWHM when the microscope stage velocity increase. The laser exposure time of the sample decrease and subsequently, the amount of metal deposited on the substrate in the same unit of time reduces proportional on speed, over 5 μm/s being imposible to have a continuous and well-defined structure.

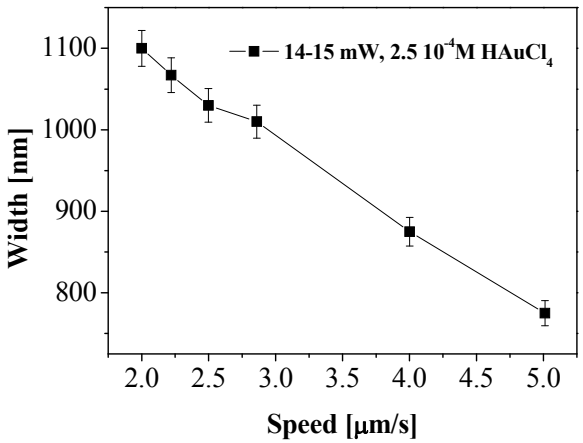

Fig. 5. Dependence of full width at half maximum of one-single wire on scanning speed

3.4 Woodpiles

Fig. 6(a) presents a 3D gold structure, fabricated by scanning the focal point in the three dimensions of the material, in the same experimental conditions employed for single-line fabrication. The 3D structure was written in a thick film with a thickness estimated at 30μm, using a 100xPh3 immersion-oil objective lens to deliver 15 mW to the sample. It is important to mention that the actual transmission of the optical microscope set-up between laser output and the focal point is 43%. That is to say that a given 15mW output of laser corresponds to 6-7mW sent at the focal point within the material.

The lines can be generated by translating the microscope stage in the XYZ-directions, at a velocity of 4 μm/s and a DT of 2 ms. The XY translation and Z displacement of the sample holder were controlled by a computer program and allowed to obtain a woodpile-like structure as quadratic prism, with 15 μm width of base along x and y axis, and 20 μm total height. The three-dimensional object consists of 10 layers. Each layer contains 7 parallel lines with a period of 2.5 μm, which are oriented alternatively, on X and Y, layer by layer. The height of each layer is about 2 μm, with a 0.2 μm step size for Z-axis and 10 integer dz-units.

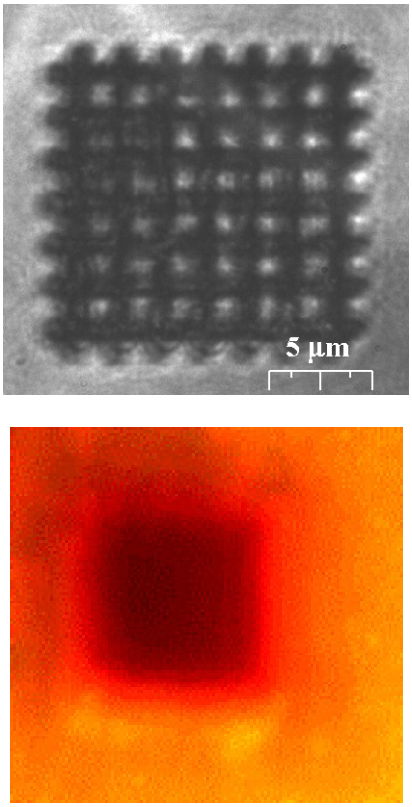

Fig. 6 Optical images of a 3D woodpile with a period of 2.5 µm, 7x7 lines per layer and 20 µm height: (a) in transmitted light with x100 oil-immersion objective; (b) in dark-field with x20 objective.

After fabrication, the unreacted matrix was removed thoroughly by washing with iso-propanol and ethanol, to leave on the substrate the three-dimensional structure, surrounded by air. But during the washing process the structure disaggregated, showing that it was actually formed from not interconnected gold nanoparticles instead of being continuous structure.

These facts gave us reason to believe that there are problems concerning the aggregation of the nanoparticles, which affects the strenght of the deposited wire. The experiments demonstrated their dependence on many factors, such as the concentration of active species, wettability and other materials properties of droplet solution, optical parameters of laser beam, and characteristics of the substrate in use. Detailed correlations between the chemical system and the technical conditions of laser-fabrication still remain to be determined.

Three-dimensional gratings are very important taking in account that a crystal lattice constitutes a structure of this type. Since the grating intervals can be mastered by this direct writing method, a photonic crystal can provide a grating suitable for use with various wavelengths. One point of importance which should be mentioned is the interpretation of the directions of the incident light which will give diffraction maxima.

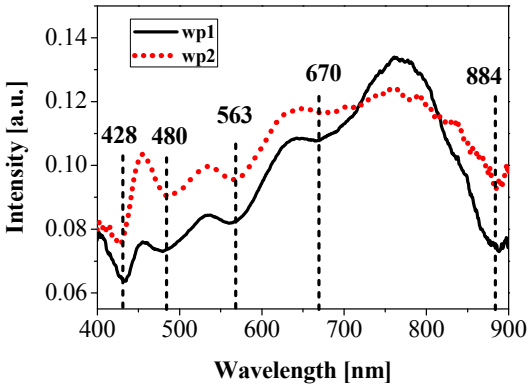

Fig. 6. Experimental transmission of the 3D grating which shows the five rejection wavelength of the structure.

Fig. 6 presents the optical diffraction (transmission under normal incidence) observed with the gold woodpile described above. It was recorded under the microscope by sampling the image plane with an optical fiber connected to a spectrometer. The two curves have been recorded at two different points of the 3D structure. They clearly exhibit five minima at five different wavelengths that can be assigned to the complex effects of transmission and reflection in the photonic crystal. These rejected wavelengths can be attributed to the reflected wavelengths of the photonic crystal structure. This behaviour is illustrated in Figure 7, where we have plotted the wavenumber $1/\lambda_B$ versus the interference order, following Bragg relation at normal incidence:

$$2nd = p \cdot \lambda_B \tag{1}$$

where $d = 2.5\ \mu m$ is the period array, $n = 1.3725$ is the refractive index of the polymer matrix and , and p is an integer giving the interference order.

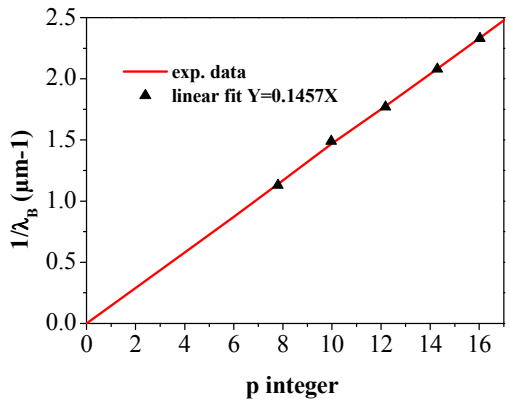

Fig. 7 Dependence of the wavenumbers associated to the rejected wavelengths versus the interference orders.

We must point out that these five rejected wavelengths correspond to the 8^{th}, 10^{th}, 12^{th}, 14^{th} and 16^{th} Bragg diffraction orders and they are in very good agreement with the calculated wavelengths. This behaviour is supported by the diffraction in gratings whose transparent and non-transparent elements have equal width, where the even order spectra are absent [19].

4. Conclusions

In this work, we developed a pathway to fabricate three-dimensional gold structures based on a metallic photo-reduction process induced by femtosecond laser irradiation. This efficient method overcomes the thermal effect pointed out by the double-line generation during the two-photon induced metal deposition. Low laser intensities generate a metallic single-wire instead of double-wire. This allowed us to fabricate well-defined three-dimensional gold microstructures within a thick film of a polymer matrix. The laser power as well as the chemical system has a significant influence on the evolution of gold nucleation and growth processes during metallic photo-reduction. The competition between nucleation and growth can explain the lack of 3D fabricated structures solidity outside of the polymer matrix, when low laser powers are employed to avoid the double-line generation.

This direct writing technique may be useful to fabricate highly efficient 3D gratings with spectral filtering properties due to the significant index contrast between polymer host and metallic parts.

Acknowledgements

We would like to acknowledge the PNANO research program of the French ANR which supported this work part of the POMESCO project.

References

[1] E. S. Wu, J. H. Strickler, W. R. Harrell, W. W. Webb, The Proc. of SPIE **1674**, 776 (1992).
[2] B. H. Cumpston, S. P. Ananthavel, S. Barlow, D. L. Dyer, J. E. Ehrlich, L. L. Erskine, A. A. Heikal, S. M. Kuebler, I.-Y. S. Lee, D. McCord-Maughon, J. Qin, H. Rockel, M. Rumi, X.-L. Wu, S. R. Marder, J. W. Perry, Nature **398**, 51 (1999).
[3] T. Baldacchini, C. LaFratta, R. A. Farrer, M. C. Teich, B. E. A. Saleh, M. J. Naughton, J. T. Fourkas, J. Appl. Phys. **95**, 6072 (2004).
[4] S. Maruro, O. Nakamura, S. Kawata, Opt. Let. **22**, 132 (1997).
[5] (a) A. N. Shipway, E. Katz, I. Willner, Chem. Phys. Chem **1**(1), 18 (2000). (b) P. Prem Kiran, B. N. Shivakiran Bhaktha, D. N. Rao, G. De, J. Appl. Phys., **96**, 6717 (2004).
[6] K. Aslan, J.R. Lakovicz, C. D. Geddes, Curr. Oppin. Chem. Biol. **9**(5), 538 (2005).
[7] P.-W. Wu, W. Cheng, I. B. Martini, B. Dunn, B. J. Schwartz, E. Yablonovitch, Adv. Mater. **12**(19), 1438 (2000).
[8] F. Stellacci, C. A. Bauer, T. Meyer-Friedrichsen, W. Wenseleers, V. Alain, S. M. Kuebler, S. J. K. Pond, Y. Zhang, S. R. Marder, J. W. Perry, Adv. Mater. **14** (3), 194 (2002).
[9] R. S. Ingram, M. J. Hostetler, R. W. Murray, J. Am. Chem. Soc. **119**(39), 9175 (1997).
[10] S. Y. Kang, K. Kim, Langmuir **14**(1) 226 (1998).
[11] T. Tanaka, A. Ishikawa, S. Kawata, The Proc. of SPIE **6324**, 1 (2006).
[12] F. Formanek, N. Takeyasu, T. Tanaka, K. Chiyoda, A. Ishikawa, S. Kawata, Opt. Expr. **14**(2), 800 (2006).
[13] J.-I. Kato, N. Takeyasu, Y. Adachi, H.-B. Sun, S. Kawata, Appl. Phys. Lett. **86**(044102), 1 (2005).
[14] F. Formanek, N. Takeyasu, T. Tanaka, K. Chiyoda, A. Ishikawa, S. Kawata, , Appl. Phys. Lett. **88**(083110), 1 (2006).
[15] N. Tosa, G. Vitrant, P. L. Baldeck, O. Stephan, S. Astilean, I. Grosu, J. Optoelectron. Adv. Mater. **9**(3), 641 (2007).
[16] N. Tosa, J. Bosson, M. Pierre, C. Rambaud, M. Bouriau, G. Vitrant, O. Stephan, S. Astilean, P. L. Baldeck, D. Andrews, The Proc. of SPIE **6195**, 1 (2006).
[17] J. Bosson-Ehoomann, A. Mihut, N. Tosa, S. Astilean, M. Pierre, C. Rambaud, L. Vurth, P. Baldeck, O. Stephan, Nonlin. Opt. Quant. Opt. **10**, 1 (2007).
[18] P. Donat, S. Panozzo, J. C. Vial, C. Beigne, R. Rieutord, Synthetic-Metals **146**(3), 225 (2004).
[19] R. S. Longhurst, Geometrical and Physical Optics, Longmans, London, 239, (1967).

*Corresponding author: nicoletatosa@gmail.com